AGN vs. quiescent galactic nuclei: Looking for synergies

CPB 2022 meeting summary

Authors: **Michal Zajaček**
Department of Theoretical Physics and Astrophysics, Faculty of Science
Masaryk University in Brno

June 3rd, 2022

Different ways to categorize galaxies/galactic nuclei

Different ways to categorize galaxies/galactic nuclei

- **morphological:** spiral, elliptical, S0, irregular
- **colour:** blue, green, red
- **radio-loud, radio-quiet or better(?) jetted/non-jetted**
- based on the ionization state (BPT narrow-line diagram, luminosity-hardness diagram)
- **with and without the Nuclear Star Cluster/Disk**
- **mass spectrum** (total stellar/halo mass)
- **viewing angle effects** (type 1, type 2 AGN...)
- **based on the intergalactic environment** (galaxy group, cluster, merging cluster)

Accretion rate as the main driver?

- accretion rate affects the properties of the accretion flow
- accretion at what radius?
- outflow-rate profile

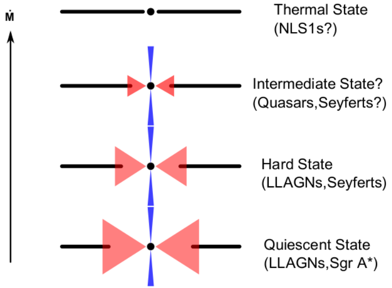

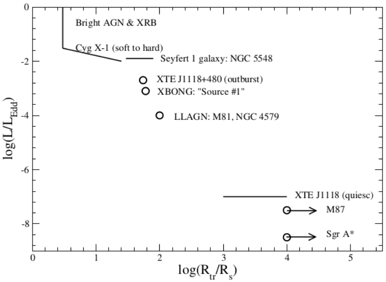

Hardness-luminosity diagram

Low/hard state vs. High/soft state for black-hole binaries

Does it apply for supermassive black holes?

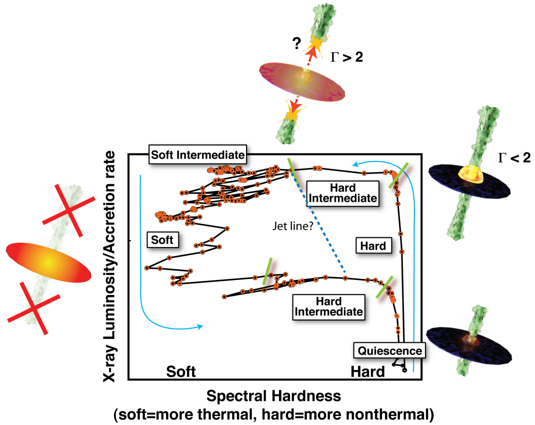

Fender et al. (2004)

High accretor vs. low accretor

Spectral energy distribution

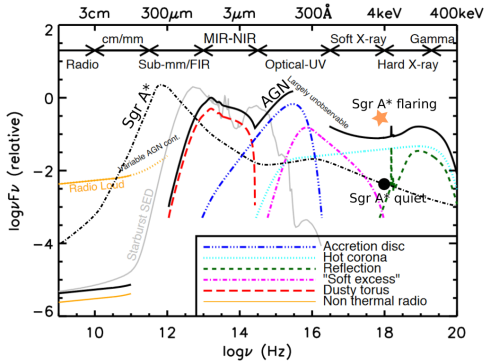

Taken from Harrison (2014)

High accretor vs. low accretor

Other trends with the accretion rate:

- the higher the accretion rate, the lower the variability

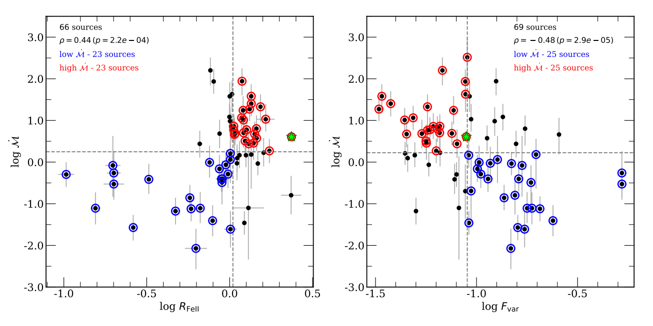

Taken from Zajacek et al. (2021)

High accretor vs. low accretor

Sgr A* is extremely low accretor, with $\dot{m} = 10^{-9} - 10^{-8}\dot{m}_{\mathrm{Edd}} \rightarrow$ high variability in the NIR and X-ray domain

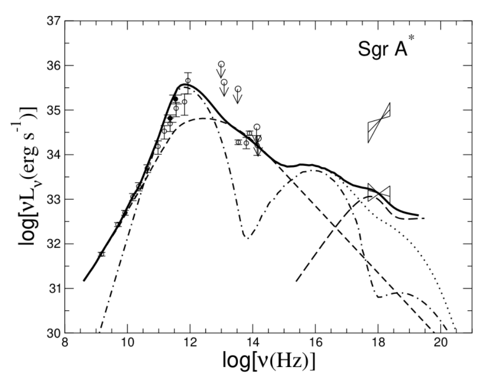

Taken from Yuan & Narayan (2014)

High accretor vs. low accretor

Flares in NIR are consistent with the toy "hot spot" model

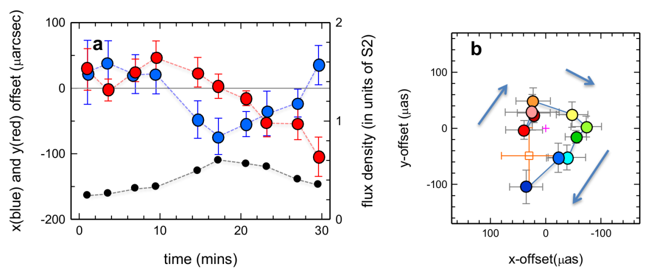

Taken from Gravity collaboration (2018)

High accretor vs. low accretor

Flares in NIR are consistent with the toy "hot spot" model

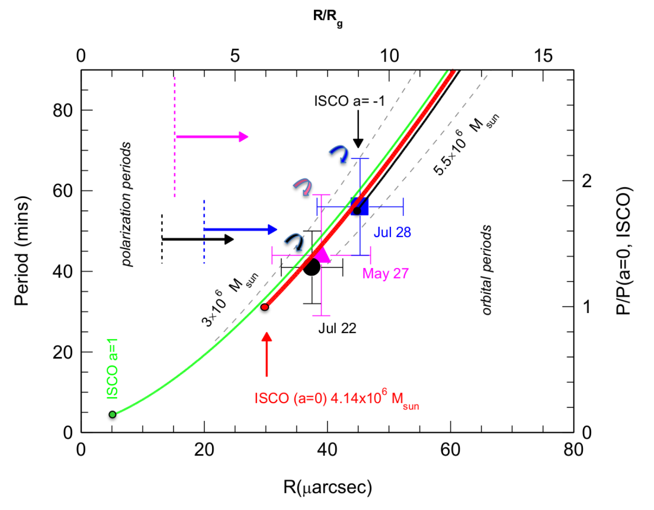

Taken from Gravity collaboration (2018)

High accretor vs. low accretor

- interesting one-to-one and one-sided correspondance between X-ray and NIR flares (every X-ray flare has a NIR counterpart but not vice-versa)
- potential distance and size(!?) dependendence of flares

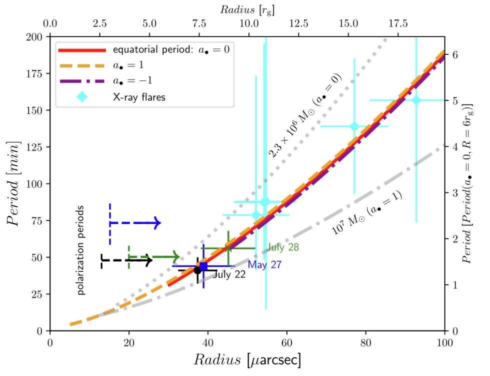

Taken from Karas et al. (2022)

AGN feedback

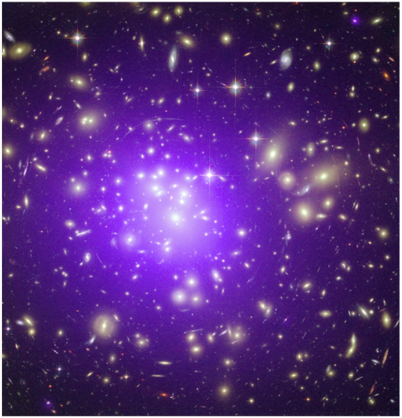

Left: Massive galaxy cluster Abell 1689; Right: Massive elliptical galaxy NGC 5813

AGN feedback

AGN feedback can operate over eight orders of magnitude: from the vicinity of the black hole to

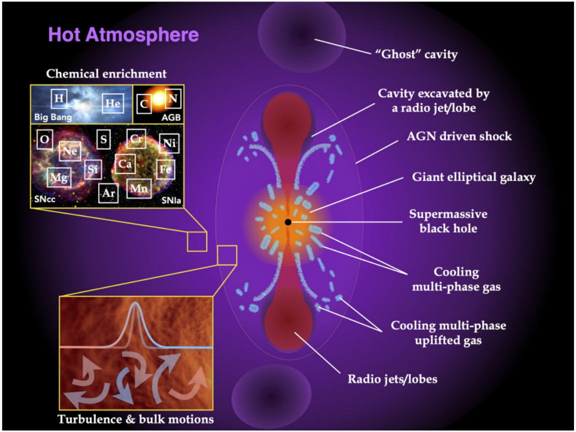

Taken from Werner & Mernier 2020

AGN feedback

Colour-mass diagram (blue cloud, red cloud, green valley)

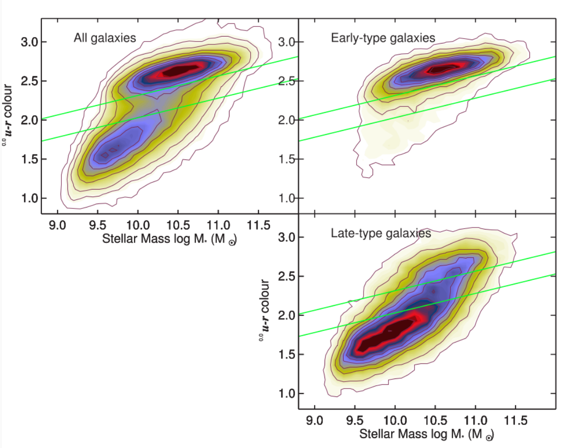

Taken from Schawinski et al. (2014)

AGN feedback

Colour-mass diagram (blue cloud, red cloud, green valley)

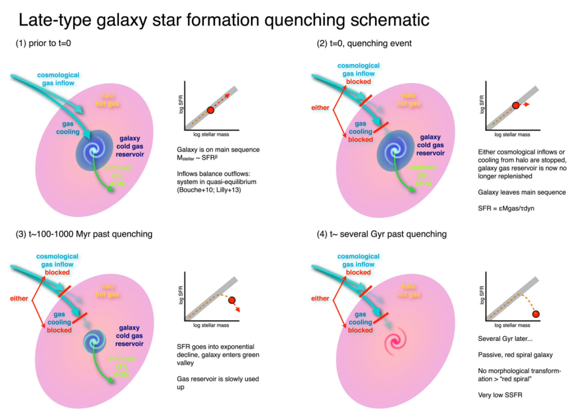

Taken from Schawinski et al. (2014)

AGN feedback

Colour-mass diagram (blue cloud, red cloud, green valley)

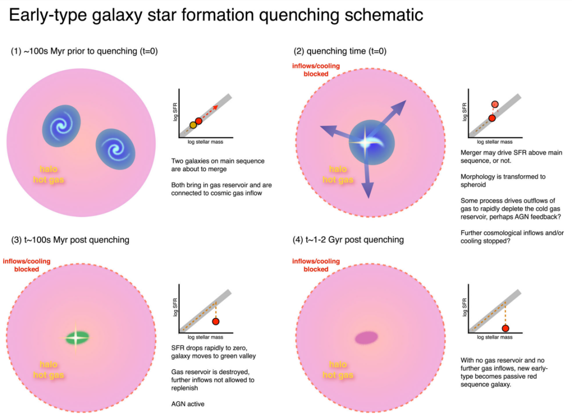

Taken from Schawinski et al. (2014)

AGN feedback

Stellar mass/halo mass as a function of the halo mass (Harrison et al. 2017)

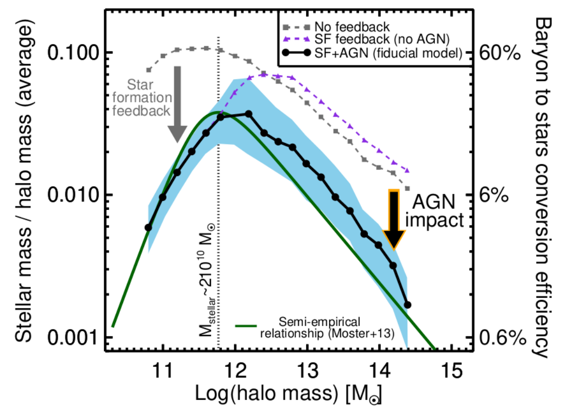

Star-formation feedback dominates for smaller halo masses, while the AGN impact is traceable at higher halo masses.

AGN feedback

During one star-formation episode ($\sim$ 100 Myr), AGN luminosity (Edd. ratio) evolves on much shorter timescales

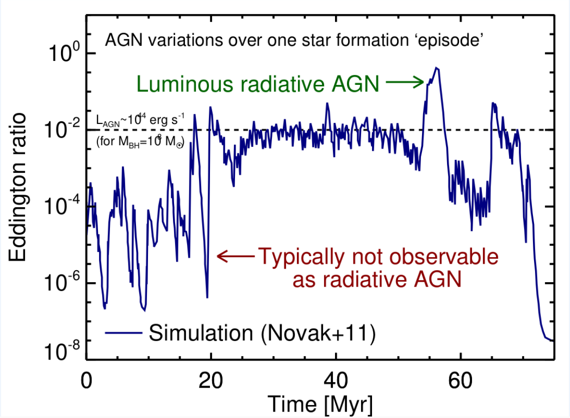

Taken from Harrison (2017)

Nuclear star clusters

- surround supermassive black holes on the scales of

$$\begin{aligned} r_{\rm NSC} &= fGM_\bullet/\sigma_\star^2 \\ &= f4.3\left(\frac{M_\bullet}{10^7\,M_\odot}\right)\left(\frac{\sigma_\star}{100\,\mathrm{km\,s^{-1}}}\right)^{-2}\ \mathrm{pc} \end{aligned}$$

- when relaxed, they should be described as Bahcall-Wolf-like density cusps fitted by a simple power-law density profile
- **Bahcall & Wolf** (1976, 1976): $n_\star \propto r^{-7/4}$ and $n_\star \propto r^{-3/2}$, even steeper for massive stellar remnants (black holes)
- densest stellar systems in galaxies

Nuclear star clusters

- surround supermassive black holes on the scales of

$$
\begin{aligned}
r_{\mathrm{NSC}} &= fGM_{\bullet}/\sigma_{\star}^{2} \\
&= f4.3\left(\frac{M_{\bullet}}{10^{7}\,M_{\odot}}\right)\left(\frac{\sigma_{\star}}{100\,\mathrm{km\,s^{-1}}}\right)^{-2}\ \mathrm{pc}
\end{aligned}
$$

- when relaxed, they should be described as Bahcall-Wolf-like density cusps fitted by a simple power-law density profile
- **Bahcall & Wolf** (1976, 1976): $n_{\star} \propto r^{-7/4}$ and $n_{\star} \propto r^{-3/2}$, even steeper for massive stellar remnants (black holes)
- densest stellar systems in galaxies

Nuclear star clusters

- surround supermassive black holes on the scales of

$$r_{\rm NSC} = fGM_\bullet/\sigma_\star^2 \\ = f4.3\left(\frac{M_\bullet}{10^7\,M_\odot}\right)\left(\frac{\sigma_\star}{100\,\mathrm{km\,s^{-1}}}\right)^{-2}\ \mathrm{pc}$$

- densest stellar systems in galaxies

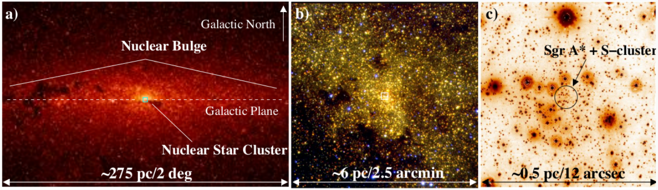

Schoedel et al. (2014)

Nuclear star clusters

- densest stellar systems in galaxies

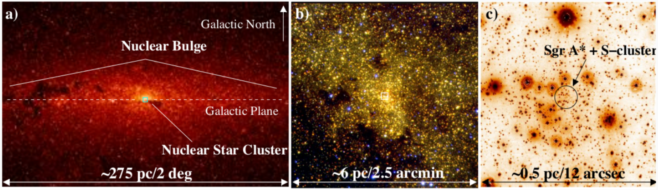

- is centered on Sgr A* and appears point-symmetric in projection;
- is flattened, with a ratio between minor and major axis of $q = 0.71 \pm 0.02$;
- has a half-light radius of $r_h = 4.2 \pm 0.4\,\mathrm{pc}$;
- has a total luminosity and mass of $L_{NSC,4.5\,\mu m} = 4.1 \pm 0.4 \times 10^7\,L_\odot$ and $M_{MW\,NSC} = 2.5 \pm 0.4 \times 10^7\,\mathrm{M}_\odot$, respectively.

Schoedel et al. (2014)

Nuclear star clusters

- occupation fraction as a function of stellar mass for early- and late-type galaxies

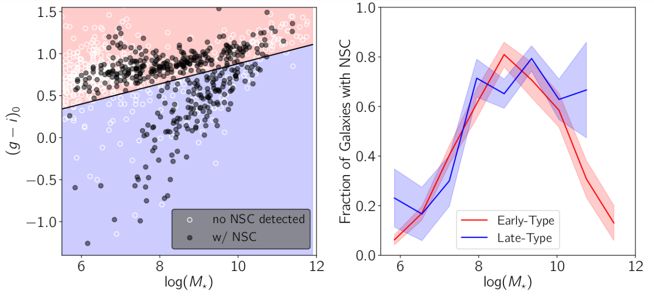

Neumayer, Seth, Böker et al. (2020)

Nuclear star clusters

- **Can "microscopic" NSCs affect the black-hole activity and AGN feedback over eight orders of magnitude in length-scale?**
- NSCs have different density profiles and a mixture of stars
- position of the **stagnation radius – inflow/outflow boundary** – is affected

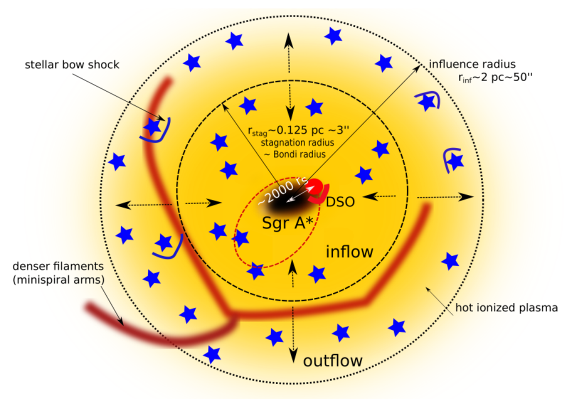

Nuclear star clusters

- position of the **stagnation radius – inflow/outflow boundary** – is affected

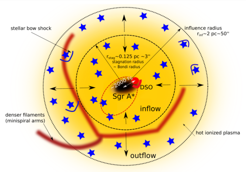

$$r_{\rm stag} \approx \left(\frac{13+8\Gamma}{4+2\Gamma} - \frac{3\nu_{\rm stag}}{2+\Gamma}\right)\frac{GM_\bullet}{\nu_{\rm stag} v_{\rm w}^2}$$

$$\approx \begin{cases} 0.30\left(\frac{M_\bullet}{4\times10^6\,M_\odot}\right)\left(\frac{v_{\rm w}}{500\,{\rm km\,s^{-1}}}\right)^{-2}\ {\rm pc} & ,\ {\rm core}\ \ (\Gamma=0.1)\,, \\ 0.16\left(\frac{M_\bullet}{4\times10^6\,M_\odot}\right)\left(\frac{v_{\rm w}}{500\,{\rm km\,s^{-1}}}\right)^{-2}\ {\rm pc} & ,\ {\rm cusp}\ \ (\Gamma=0.8)\,, \end{cases} \tag{8}$$

where Γ is the power-law index of the inner stellar brightness profile. For estimative purposes, we consider two limiting cases, the core profile with $\Gamma = 0.1$ and the stellar cusp with $\Gamma = 0.8$. The quantity $\nu_{\rm stag} = -{\rm d}n_{\rm a}/{\rm d}r|_{r_{\rm stag}}$ is the gas density power-law slope at $r_{\rm stag}$, which according to the numerical analysis of Generozov et al. (2015) is $\nu_{\rm stag} \approx 1/6[(4\Gamma+3)]$. According to the estimates in Eq. (8), the stagnation radius is expected to be located close to the Bondi radius with an offset given by the numerical factor (Generozov et al., 2015)

$$\frac{r_{\rm stag}}{r_{\rm B}} \approx \frac{13+8\Gamma}{(2+\Gamma)(3+4\Gamma)}\,, \tag{9}$$

which is of the order of unity. This is also illustrated in the two-zone scheme in Fig. 2.

Nuclear star clusters

- position of the **stagnation radius – inflow/outflow boundary** – is affected

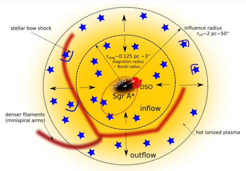

$$
\begin{aligned}
r_{\rm stag} &\approx \left(\frac{13+8\Gamma}{4+2\Gamma} - \frac{3\nu_{\rm stag}}{2+\Gamma}\right)\frac{GM_\bullet}{\nu_{\rm stag} v_{\rm w}^2} \\
&\approx \begin{cases} 0.30\left(\frac{M_\bullet}{4\times10^6\,M_\odot}\right)\left(\frac{v_{\rm w}}{500\,{\rm km\,s^{-1}}}\right)^{-2}\,{\rm pc} & \text{, core } (\Gamma=0.1)\,, \\ 0.16\left(\frac{M_\bullet}{4\times10^6\,M_\odot}\right)\left(\frac{v_{\rm w}}{500\,{\rm km\,s^{-1}}}\right)^{-2}\,{\rm pc} & \text{, cusp } (\Gamma=0.8)\,, \end{cases}
\end{aligned}
\tag{8}
$$

where Γ is the power-law index of the inner stellar brightness profile. For estimative purposes, we consider two limiting cases, the core profile with $\Gamma = 0.1$ and the stellar cusp with $\Gamma = 0.8$. The quantity $\nu_{\rm stag} = -{\rm d}n_{\rm a}/{\rm d}r|_{r_{\rm stag}}$ is the gas density power-law slope at $r_{\rm stag}$, which according to the numerical analysis of Generozov et al. (2015) is $\nu_{\rm stag} \approx 1/6[(4\Gamma+3)]$. According to the estimates in Eq. (8), the stagnation radius is expected to be located close to the Bondi radius with an offset given by the numerical factor (Generozov et al., 2015)

$$
\frac{r_{\rm stag}}{r_{\rm B}} \approx \frac{13+8\Gamma}{(2+\Gamma)(3+4\Gamma)}\,, \tag{9}
$$

which is of the order of unity. This is also illustrated in the two-zone scheme in Fig. 2.

Nuclear star clusters

- position of the **stagnation radius – inflow/outflow boundary** – is affected
- sources with **no NSC/core-like NSC** $\rightarrow$ a bigger potential for **the AGN/high-accretion mode** since $r_{\rm stag}$ is big and the matter inside $\sim r_{\rm stag}^3$ can accummulate for massive black holes?
- **cusp-like NSC may prohibit the accummulation of a large amount of matter** $\rightarrow$ quiescent/Milky Way-like ADAF mode?

$$
\begin{aligned}
r_{\rm stag} &\approx \left(\frac{13+8\Gamma}{4+2\Gamma}-\frac{3\nu_{\rm stag}}{2+\Gamma}\right)\frac{GM_\bullet}{\nu_{\rm stag}v_{\rm w}^2} \\
&\approx \begin{cases} 0.30\left(\frac{M_\bullet}{4\times10^6\,M_\odot}\right)\left(\frac{v_{\rm w}}{500\,{\rm km\,s^{-1}}}\right)^{-2}\,{\rm pc} & ,\ {\rm core}\ (\Gamma=0.1)\,, \\ 0.16\left(\frac{M_\bullet}{4\times10^6\,M_\odot}\right)\left(\frac{v_{\rm w}}{500\,{\rm km\,s^{-1}}}\right)^{-2}\,{\rm pc} & ,\ {\rm cusp}\ (\Gamma=0.8)\,, \end{cases}
\end{aligned}
\tag{8}
$$

where Γ is the power-law index of the inner stellar brightness profile. For estimative purposes, we consider two limiting cases, the core profile with $\Gamma = 0.1$ and the stellar cusp with $\Gamma = 0.8$. The quantity $\nu_{\rm stag} = -{\rm d}n_{\rm a}/{\rm d}r|_{r_{\rm stag}}$ is the gas density power-law slope at $r_{\rm stag}$, which according to the numerical analysis of Generozov et al. (2015) is $\nu_{\rm stag} \approx 1/6[(4\Gamma+3)]$. According to the estimates in Eq. (8), the stagnation radius is expected to be located close to the Bondi radius with an offset given by the numerical factor (Generozov et al., 2015)

$$
\frac{r_{\rm stag}}{r_{\rm B}} \approx \frac{13+8\Gamma}{(2+\Gamma)(3+4\Gamma)}\,, \tag{9}
$$

which is of the order of unity. This is also illustrated in the two-zone scheme in Fig. 2.

What to look for?

- JWST results (first image July 12)
- IXPE (completely new information)
- ELT: METIS, MICADO
- Athena - maybe a problem...
- LISA

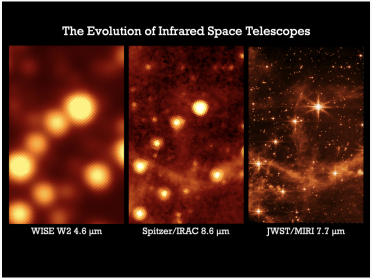

Meeting photos

Meeting photos

Meeting photos

Meeting photos

Meeting photos

Meeting photos

Meeting photos

Meeting photos

Texas Symposium in Prague

- 31st Texas Symposium conference
- **September 12-16 2022 in Prague**

Friday evening

- **18:30** Jean-Paul's restaurant (30 places) - order yourself (**Běhounská 4**)
- **21:00** Air Café (**Zelný trh 8**)

Saturday – relaxed sightseeing

- **10:00** meeting close to the Brno black astronomical clock (Náměstí Svobody)
- some people may go **bouldering**: talk to Kristína Kallová

Future

See you at next “CP” meeting in Cologne, Prague
or elsewhere